RESEARCH ARTICLE OPEN ACCESS

Analysis of Key Differential Metabolites in Intervertebral Disc Degeneration Based on Untargeted Metabolomics

Daqian Zhou[1] | Xingrui Zhang[2] | Jiale Lv[1] | Yongliang Mei[1] | Yingjin Luo[1] | Fengjiang Li[1] | Zongchao Liu[1,3]

[1]Department of Orthopedics, The Affiliated Traditional Chinese Medicine Hospital, Southwest Medical University, Luzhou, Sichuan, China | [2]Department of Orthopedics, The First People's Hospital of Liangshan YiAutonomous Prefecture, Liangshan, Sichuan, China | [3]Luzhou Longmatan District People's Hospital, Luzhou, Sichuan, China

Correspondence: Zongchao Liu (lzcxnykdx@swmu.edu.cn)

Received: 23 September 2024 | **Revised:** 19 November 2024 | **Accepted:** 13 December 2024

Funding: This work was supported in part by research grants from the Program for Luzhou Municipal People's Government-Southwest Medical University Science and Technology Strategic Cooperation Climbing Project (2021LZXNYD-D02), Luzhou City Science and Technology Research and Development Projects (2022-SYF-42), Sichuan Provincial Science and Technology Plan Joint Innovation Special Project (2022YFS0609-B3), and Luzhou City Science and Technology Innovation Seedling Cultivation Plan (2022-RCM-178).

Keywords: intervertebral disc degeneration | IVDD | metabolic marker | nontargeted metabolomics | UHPLC-MS

ABSTRACT

Background: Intervertebral disc degeneration disease (IVDD) is a prevalent orthopedic condition that causes chronic lower back pain, imposing a substantial economic burden on patients and society. Despite its high incidence, the pathophysiological mechanisms of IVDD remain incompletely understood.

Objective: This study aimed to identify metabolomic alterations in IVDD patients and explore the key metabolic pathways and metabolites involved in its pathogenesis.

Methods: Serum samples from 20 IVDD patients and 20 healthy controls were analyzed using ultra-high-performance liquid chromatography-mass spectrometry (UHPLC–MS). The identified metabolites were mapped to metabolic pathways using the Kyoto Encyclopedia of Genes and Genomes (KEGG) database.

Results: Significant alterations were observed in metabolites such as 2-methyl-1,3-cyclohexadiene, stearoyl sphingomyelin, methylcysteine, L-methionine, and cis, cis-muconic acid. These metabolites were involved in pathways including glycine, serine, and threonine metabolism, cyanoamino acid metabolism, and the citrate cycle (TCA cycle).

Conclusion: The identified metabolic alterations provide insights into the pathogenesis of IVDD and suggest potential therapeutic targets for future investigation.

1 | Introduction

The intervertebral disc degeneration (IVDD) is the largest lack of vascular tissue in the human body, mainly composed of three parts: the central nucleus pulposus (NP) tissue, the annulus fibrosus (AF) on both sides, and the upper and lower cartilaginous endplates(CEP), and nutrients and metabolites mainly enter and exit through the semipermeable membranous pores in the cartilaginous plates [1]. IVDD is a common and difficult-to-treat orthopedic degenerative disease, and lower back pain (LBP) is the most common symptom in patients with IVDD, affecting about 40% of the global population [2], which not only reduces people's quality of life, but also puts a heavy burden on the social healthcare system [3]. Its pathophysiology is unclear, but potential cellular molecular mechanisms include oxidative stress, senescence, apoptosis and pyroptosis

Daqian Zhou and Xingrui Zhang contributed to the work equally and should be regarded as cofirst authors.

of nucleus pulposus cells (NPCs), mechanical injury, and the aggregation of inflammatory substances brought on by a variety of circumstances [4–6]. Clinical IVDD treatment is mainly based on surgery and conservative treatment [7], and conservative treatment includes the application of hormones, anti-inflammatory drugs, and massage and acupressure techniques, which can alleviate the pain symptoms to a certain extent in the early stage of the disease [8]. Surgical treatment mainly relieves lower back pain by removing the protruding nucleus pulposus, but it is still plagued by a high recurrence rate, heavy economic burden and serious adverse events [9]. Therefore, an in-depth understanding of its pathogenesis and the discovery of new therapeutic targets for the prevention and treatment of IVDD have become an urgent need.

Metabolomics is a new scientific entity used to study life activities after genomics and proteomics, and in addition to genomics, metabolomics reflects the effects of environmental exposures [10]. Metabolomics studies small molecule metabolites (molecular weight < 1500 Da) that are more directly related to phenotype [11], and exploring the pathogenesis of complex diseases through metabolomics is an attractive area of research. Therefore, measuring changes in serum metabolomics during pathology is a good strategy to study IVDD diseases. In the present study, we used ultra-high performance liquid chromatography tandem mass spectrometry (UHPLC/MS) to detect serum differential metabolites in the normal control group and the IVDD disease group, and we identified significant alterations in 23 metabolites, KEGG analysis revealed that these metabolites are associated with pathways such as glycine, serine, and threonine metabolism, cyanoamino acid metabolism, the citrate cycle (TCA cycle), and aminoacyl-tRNA biosynthesis. These findings suggest potential roles for these pathways in the pathogenesis of IVDD.

2 | Materials and Methods

2.1 | Source of Research Subjects

All IVDD patients were inpatients from the Affiliated Hospital of Traditional Chinese Medicine of Southwest Medical University. All patients were equally divided between men and women, with a BMI in the normal range (18.5–24 kg/m^2), and the control group was matched to the IVDD group. Twenty patients with Pfirrmann disc degeneration grade III or higher were selected into the IVDD disease group according to the modified Pfirrmann disc degeneration grading [12, 13], and all patients with IVDD were in the stabilization stage defined by the Kirkcaldy–Willis and Farfan staging [14]. Twenty normal controls were selected from the Physical Examination Center of the Affiliated Hospital of Traditional Chinese Medicine of Southwest Medical University or poster recruitment. The study was reviewed and approved by the Medical Ethics Committee of the Affiliated Hospital of Traditional Chinese Medicine of Southwest Medical University [KY2021051-FS01], and the samples and clinical information of the subjects were collected after obtaining their informed consent. The following exclusion criteria were used: (1) those with mental abnormality, incapacity for autonomous behavior, and noncooperation with clinical observation and treatment. (2) Patients with severe primary diseases such as diabetes, gout, enteritis and hematopoietic system. (3) Patients with gastrointestinal resection or partial resection. (4) Patients with tumor diseases. (5) Patients who are unwilling to cooperate with the study.

2.2 | Sample Collection

We collected 2–4 mL of whole blood from fasting participants at 7:00 a.m. under standardized conditions. Blood was drawn from the cubital vein into tubes with no additives. After allowing the blood to coagulate and stratify at room temperature for 1 h, it was centrifuged at 3000 rpm for 10 min at room temperature. The resulting supernatant was further centrifuged at 12000 rpm for 10 min at 4°C to remove any remaining cellular debris. The final plasma was aliquoted into 1.5 mL tubes (0.2 mL per tube) and stored at −80°C until further analysis.

Our study chose to analyze plasma metabolites as opposed to those extracted from isolated cells, which is more common in IVDD-related metabolomic studies. Plasma metabolomics offers several advantages, including its minimally invasive nature and ability to reflect systemic metabolic changes, which is critical for identifying potential biomarkers. However, it does have limitations, such as being influenced by external factors unrelated to IVDD. In contrast, analyzing metabolites from isolated nucleus pulposus (NP) cells or intervertebral disc tissue allows for more direct insights into local metabolic alterations but requires invasive sample collection [15, 16].

2.3 | Metabolite Extraction

The serum samples stored at −80°C were melted and 100 μL of sample was transferred to an EP tube. After the addition of 400 μL of extract solution (methanol:acetonitrile = 1:1, containing isotopically-labeled internal standard mixture), the samples were vortexed for 30 s, sonicated for 10 min in ice-water bath, and incubated for 1 h at −40°C to precipitate proteins. Then the sample was centrifuged at 12000 rpm (RCF = 13 800(×*g*), *R* = 8.6 cm) for 15 min at 4°C. The resulting supernatant was transferred to a fresh glass vial for analysis. The quality control (QC) sample was prepared by mixing an equal aliquot of the supernatants from all of the samples [17].

2.4 | LC–MS/MS Analysis

LC–MS/MS analyses were performed using an UHPLC system (Vanquish, Thermo Fisher Scientific) with a UPLC BEH Amide column (2.1 mm × 100 mm, 1.7 μm) coupled to Orbitrap Exploris 120 mass spectrometer (Orbitrap MS, Thermo). The mobile phase consisted of 25 mmol/L ammonium acetate and 25 ammonia hydroxide in water (pH = 9.75) (A) and acetonitrile (B). The auto-sampler temperature was 4°C, and the injection volume was 2 μL. The Orbitrap Exploris 120 mass spectrometer was used for its ability to acquire MS/MS spectra on information-dependent acquisition (IDA) mode in the control of the acquisition software (Xcalibur, Thermo). In this mode, the acquisition software continuously evaluates the full scan MS spectrum. The ESI source conditions were

set as following: sheath gas flow rate as 50 Arb, Aux gas flow rate as 15 Arb, capillary temperature 320°C, full MS resolution as 60 000, MS/MS resolution as 15 000 collision energy as 10/30/60 in NCE mode, spray voltage as 3.8 kV (positive) or −3.4 kV (negative), respectively [18].

2.5 | Preprocessing of Mass Spectrometry Raw Data and Identification of Metabolites

Mass spectrometry (MS) raw data files were converted to Extensible Markup Language (mzXML) format by the proteo wizard. The "XCMS" R package v3.2 was used for the following processes: peak inverse plethysmography, alignment, and integration. mbidiac and cutoff values were set to 0.5 and 0.3, respectively. The metabolite identification methods used included m/z spectroscopy, retention time, and secondary ion fragmentation. The retention time (RT) of the substance was obtained by chromatographic separation, and the primary parent ion and secondary fragment ion information of the substance was obtained by mass spectrometric detection. The detected mass spectrometry information was matched with the secondary mass spectrometry database established by BiotreeDB to annotate the metabolites. The identification criteria Δ values were ±30 s and ppm (mass accuracy) ±10. In the characterization results, the scoring values of the secondary characterized metabolites were calculated based on Euclidean distance and dot product algorithms [19, 20]. The cut-off value of the algorithm was set as 0.3.

2.6 | Principal Component Analysis

Metabolomic data, due to its high-throughput nature, represents a multivariate dataset where each compound corresponds to a specific data dimension. Principal Component Analysis (PCA) was performed as an initial exploratory step to analyze the data. PCA is a statistical method that uses orthogonal transformation to convert a set of potentially correlated variables into a set of linearly uncorrelated variables, referred to as principal components [21].

As an unsupervised model, PCA reveals the internal structure of the data, reduces dimensionality, and retains the most informative features of the original dataset using a smaller number of principal components.

In this study, PCA was applied to visualize the global distribution patterns of metabolomic data in a two-dimensional or three-dimensional space. This approach effectively highlighted the overall trends and differences between sample groups. However, as PCA is an unsupervised model, it may be influenced by variables unrelated to grouping information, limiting the clarity of intergroup differences. To address this, we employed a supervised classification model, OPLS-DA, for more distinct group separation, as described in the following section. Both PCA and OPLS-DA analyses were performed using SIMCA software (V16.0.2, Sartorius Stedim Data Analytics AB, Umea, Sweden) after logarithmic (LOG) transformation and centering (CTR) [22].

2.7 | Orthogonal Partial Least Squares-Discriminant Analysis

Metabolomic data are characterized by high dimensionality and complex correlations among variables, which may obscure the detection of meaningful group differences. To address this, we applied orthogonal partial least squares-discriminant analysis (OPLS-DA), a supervised statistical method that separates orthogonal variables (unrelated to classification) from non-orthogonal variables (related to classification). This approach enhances the identification of differential metabolites associated with the experimental groups [23]. Data preprocessing, including logarithmic (log) transformation and unit variance (UV) scaling, was performed using SIMCA software (V16.0.2, Sartorius Stedim Data Analytics AB, Umea, Sweden). OPLS-DA modeling was conducted to evaluate group separation, followed by 7-fold cross-validation to assess the model's interpretability (R^2Y) and predictive ability (Q^2). Permutation tests were used to confirm the robustness of the model by generating random Q^2 values through multiple reshufflings of the categorical variable order.

2.8 | Bioinformatic Analysis

Data from positive and negative ion modes were combined during the analysis. Results are expressed as mean ± SEM. One-way statistical analyses were performed using Student's *t*-tests, with p values < being 0.05, and differences were considered statistically significant. Differential metabolites were screened by multivariate statistical analysis using latent structure discriminant analysis (OPLS-DA) and two criteria (VIP value > 1 and p value < 0.05) [24, 25]. Differential metabolites were mapped to the KEGG database (https://www.genome.jp/kegg/) for pathway and network analysis [26]. All the characteristic peaks detected were used for OPLS DA, while the volcano plots, pathway analysis, and network analysis were based on the characteristic peaks with annotations (metabolites).

3 | Result

3.1 | PCA Analysis of Control and Model Groups

The PCA score scatter plot (Figure 1A) effectively distinguishes the normal control group from the IVDD disease group. The first two principal components, PC [1] and PC [2], respectively, reveal significant group-level differences in metabolite profiles. Each scatter represents a sample, with closer distributions indicating similar metabolic profiles and more distant distributions reflecting greater metabolic variation.

The 3D scatterplot (Figure 1B) further emphasizes the distinct clustering of the two groups within the 95% confidence interval (Hotelling's *T*-squared ellipse). This clear separation highlights differences in metabolite profiles between the normal control and IVDD disease groups, suggesting underlying metabolic alterations associated with IVDD.

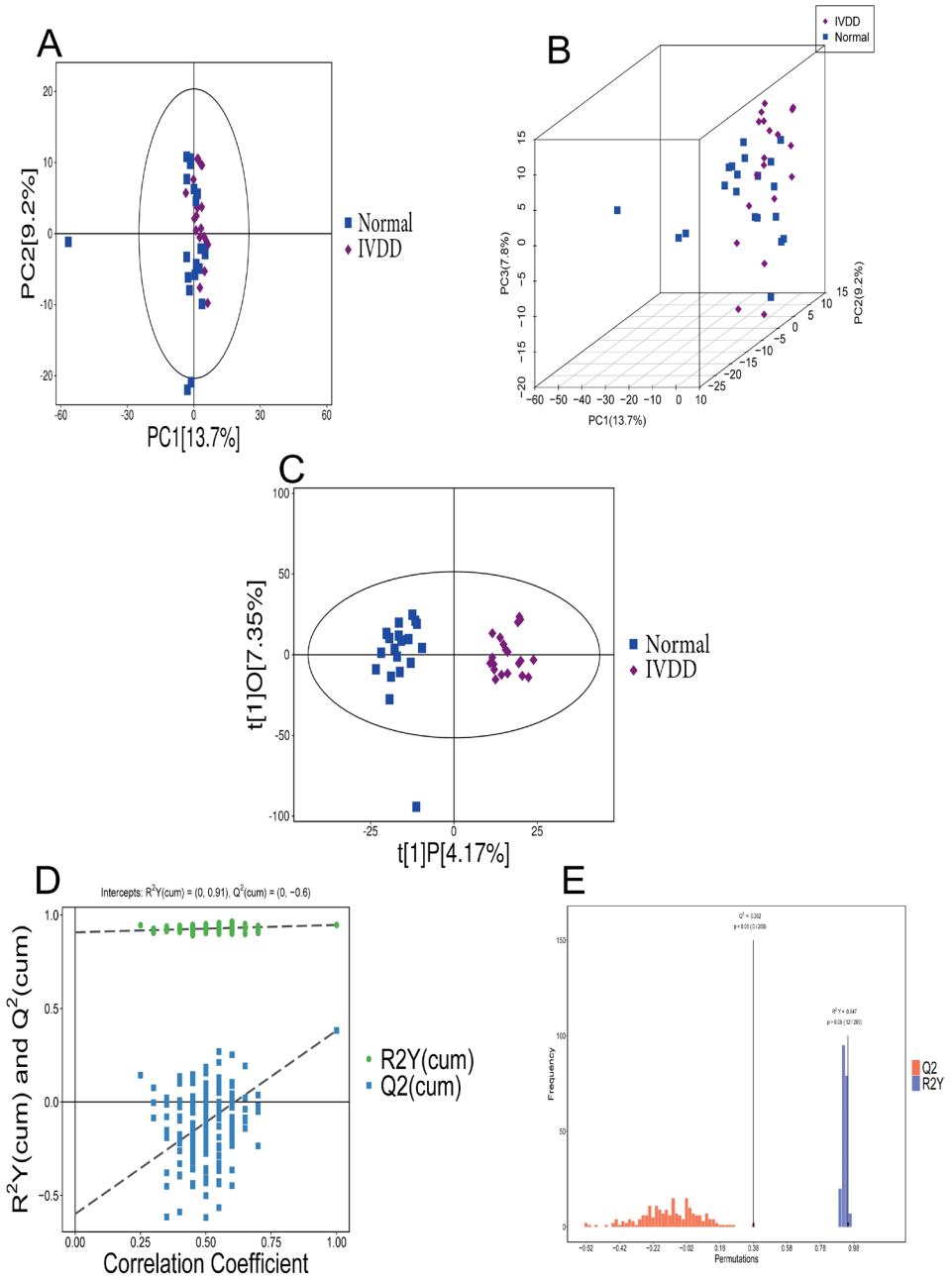

FIGURE 1 | Scatter plots of the OPLS-DA scores and OPLS-DA permutation plot. (A) The PCA score scatter plot of the normal control group and the IVDD disease group. (B) The scatterplot of the 3D scores of the normal control group and the IVDD disease group. (C) The scatter plot of the OPLS-DA model scores for the normal control group versus the IVDD disease group. (D) The dot plot of the replacement test results of the OPLS-DA model for the control group versus the IVDD group. (E) Histogram of the results of the replacement test for the OPLS-DA model for the control versus IVDD group.

3.2 | Scatterplot of OPLS-DA Scores With Permutation Test

The OPLS-DA score scatter plot comparing the normal control and IVDD groups is shown in (Figure 1C). The horizontal axis, $t[1]P$, represents the predicted principal component score, illustrating inter-group differences, while the vertical axis, $t[1]O$, represents orthogonal principal component scores, indicating intra-group variations. Each scatter point corresponds to a sample, with different colors and shapes distinguishing experimental subgroups. A greater horizontal distance between samples signifies larger intergroup differences, while closer vertical distances indicate better within-group consistency.

Figure 1D highlights the variable importance in projection (VIP) scores of the top-ranked features driving group separation. Key features with high correlations (e.g., *X* and *Y*) and low correlations (e.g., *A* and *B*) are annotated in the figure. These features represent metabolites with significant contributions to the model's predictive accuracy, providing insights into potential biomarkers for IVDD.

Permutation testing, conducted by randomly shuffling categorical variable Y multiple times ($n = 200$), evaluates the model's statistical significance and robustness against overfitting. Results of the permutation test for the OPLS-DA model are shown in (Figure 1E). The horizontal axes indicate retention of the original model's categorical variables, and vertical axes indicate R^2Y and Q^2 values. Green dots represent R^2Y values, blue squares represent Q^2 values, and dashed lines depict regression trends for both metrics.

The histogram in Figure 1F further supports the validity of the model, showing that the original model significantly outperforms random permutations with a p value < 0.05. These findings underscore the robustness of the OPLS-DA model and its ability to identify meaningful group distinctions based on metabolite profiles.

3.3 | Screening for Differential Metabolites and Volcano Maps

After the above analysis, combined with the results of univariate and multivariate statistical analysis, the differential metabolites were screened out (Table S1), and the volcano plot can visualize the overall distribution of metabolite differences between the groups, and we visualized the results of the screening of differential metabolites in the form of a volcano plot (volcano plot). The results of the control group versus the IVDD group are shown in (Figure 2A): each point in the volcano plot represents a peak, and the plot contains all the substances measured in this experiment. The horizontal coordinate represents the fold change of the group comparing each substance (taking the logarithm of the base 2), the vertical coordinate represents the p value of the student's t-test (taking the negative of the logarithm of the base 10), and the size of the scatter represents the VIP value of the OPLS-DA model, with the larger scatter being the larger the VIP value. Significantly up-regulated metabolites are shown in red, significantly down-regulated metabolites are shown in blue, and nonsignificantly different metabolites are gray. The Z-score plot of the differential metabolites is shown in (Figure 2B): the Z-score plot is in the normalization of the differential metabolites in different samples by calculating the Z-score value, the horizontal coordinate indicates the Z value, the vertical coordinate indicates the differential metabolites, and the dots of different colors indicate the samples of different groups, so that we can see the distribution of each differential metabolite among different groups very intuitively, and the specific formula is $z = (x - \mu)/\sigma$: where x is a specific score, μ is the mean, and σ is the standard deviation.

3.4 | Hierarchical Cluster Analysis of Differential Metabolites

Through the analysis of the above basic data, a series of bioinformatics analyses of significantly different metabolites are still needed, and the results are better visualized and presented. The screened differential metabolites often exhibit biological similarity/complementarity in outcome and function or are positively/negatively regulated by the same metabolic pathway. This is reflected in similar or opposite expression characteristics among different experimental groups.

Hierarchical clustering analysis of such features helps group metabolites with similar characteristics together and reveals variations in metabolite expression among experimental groups. We calculated the Euclidean distance matrix (EDM) for the quantitative values of the differential metabolites, clustered the differential metabolites using a complete chaining approach, and presented the results in a heatmap (Figure 2C). The heatmap now includes color labels to distinguish the experimental groups: blue represents the control group, and red represents the IVDD group. This labeling provides a clearer visual representation of the groupings and highlights distinct patterns of metabolite expression between groups. Differential metabolites with similar expression patterns are clustered together, aiding in the identification of key metabolic variations associated with IVDD.

3.5 | Boxplot, Matchstick Plot and Radargram Analysis of Differential Metabolites

Boxplots were utilized to display the distribution characteristics and variability of differential metabolites between the control and IVDD groups (Figure 3). To ensure accuracy and avoid arbitrary connections, all metabolite values were normalized prior to plotting. Normalization involved scaling the quantitative data for each metabolite to a range of [0,1] based on the minimum and maximum values within the dataset. Each axis in the radar plot represents a unique metabolite, and the gridlines reflect normalized fold changes. The purple shading connects the normalized values of the metabolites, providing an intuitive visualization of relative abundance trends across groups. This approach highlights key differences while ensuring that the connections between metabolites are statistically meaningful. Statistical significance was determined using Student's t-test or ANOVA, with a p value < 0.05 considered significant.

For further analysis, the quantitative values of differential metabolites were log-transformed (base 2), and the top 15 upregulated and downregulated metabolites with the largest fold changes were selected (Figure 4A). In the matchstick plot, the x-axis represents the log-transformed fold changes, and the color intensity of each point corresponds to its VIP value, highlighting metabolites with significant changes.

The radar plot (Figure 4B) visualizes the trend changes in differential metabolite content. Each grid line represents a fold change, and the purple shading connects the fold changes of individual metabolites, providing an intuitive overview of their variations between groups.

3.5.1 | Correlation Analysis of Differential Metabolites

Although certain metabolic pathways may have predictable, fixed patterns, the correlations between metabolites can still reveal potential synergistic changes that suggest regulatory relationships in biological states. We used Pearson's method to calculate the correlation coefficients between the quantitative

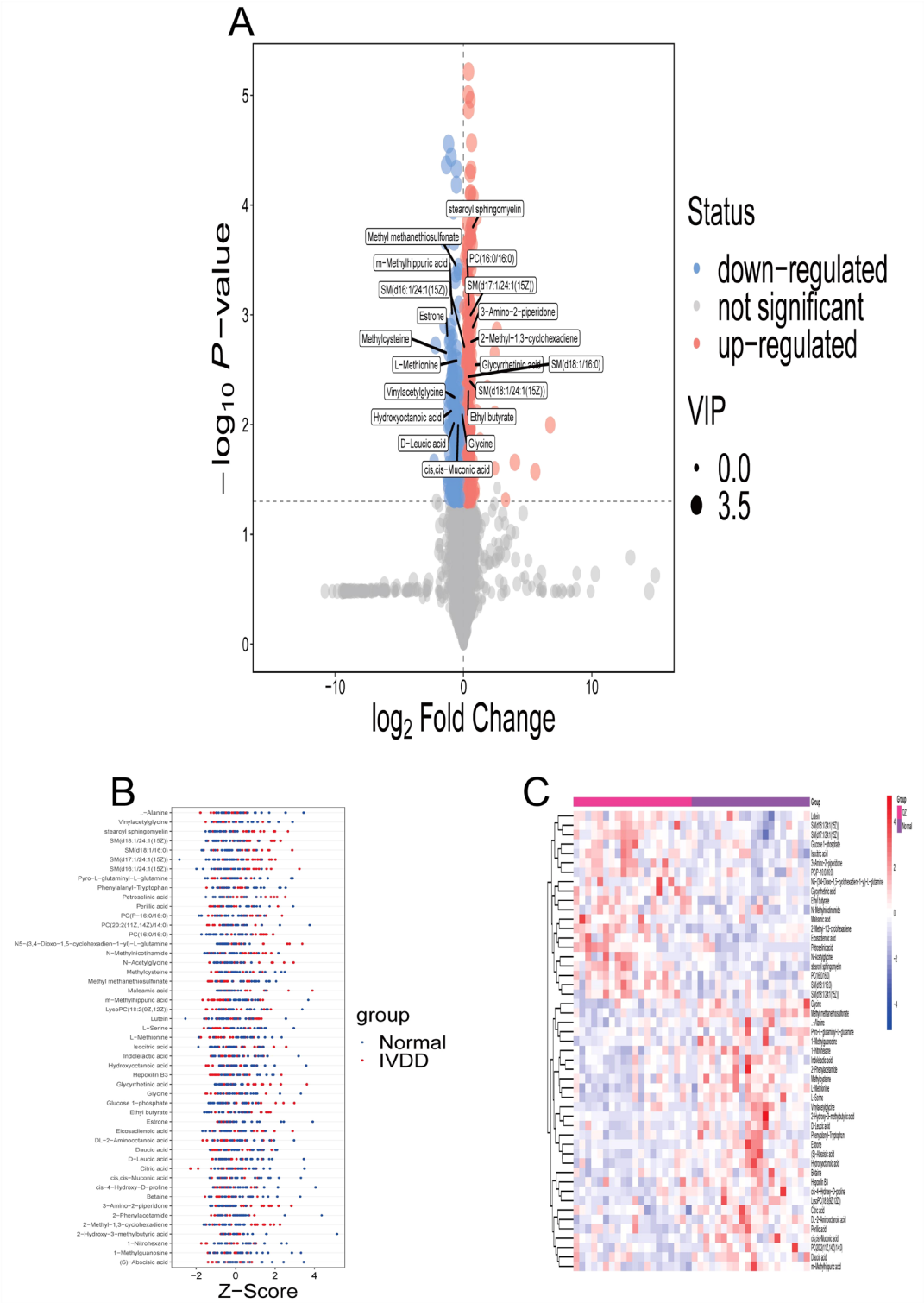

FIGURE 2 | Screening for differential metabolites. (A) The differential metabolites in the form of a volcano plot. (B) The *Z*-score plot of the differential metabolites. (C) Hierarchical cluster analysis of differential metabolites in the control group and the IVDD group in a heat map.

values of the differential metabolites and presented the results in a heatmap (Figure 4C) [27]. In the heatmap, the horizontal and vertical axes represent the differential metabolites. The color blocks indicate the strength of the correlation coefficients between the metabolites, with red representing positive correlations and blue representing negative correlations. Darker colors indicate stronger correlations. Significant correlations are marked with an asterisk (*). We further discussed the potential biological mechanisms behind these strong correlations in the revised discussion section.

3.5.2 | Chordal Analysis of Differential Metabolites

Figure 4D presents a chordal analysis of differential metabolites, which illustrates the relationships between metabolite

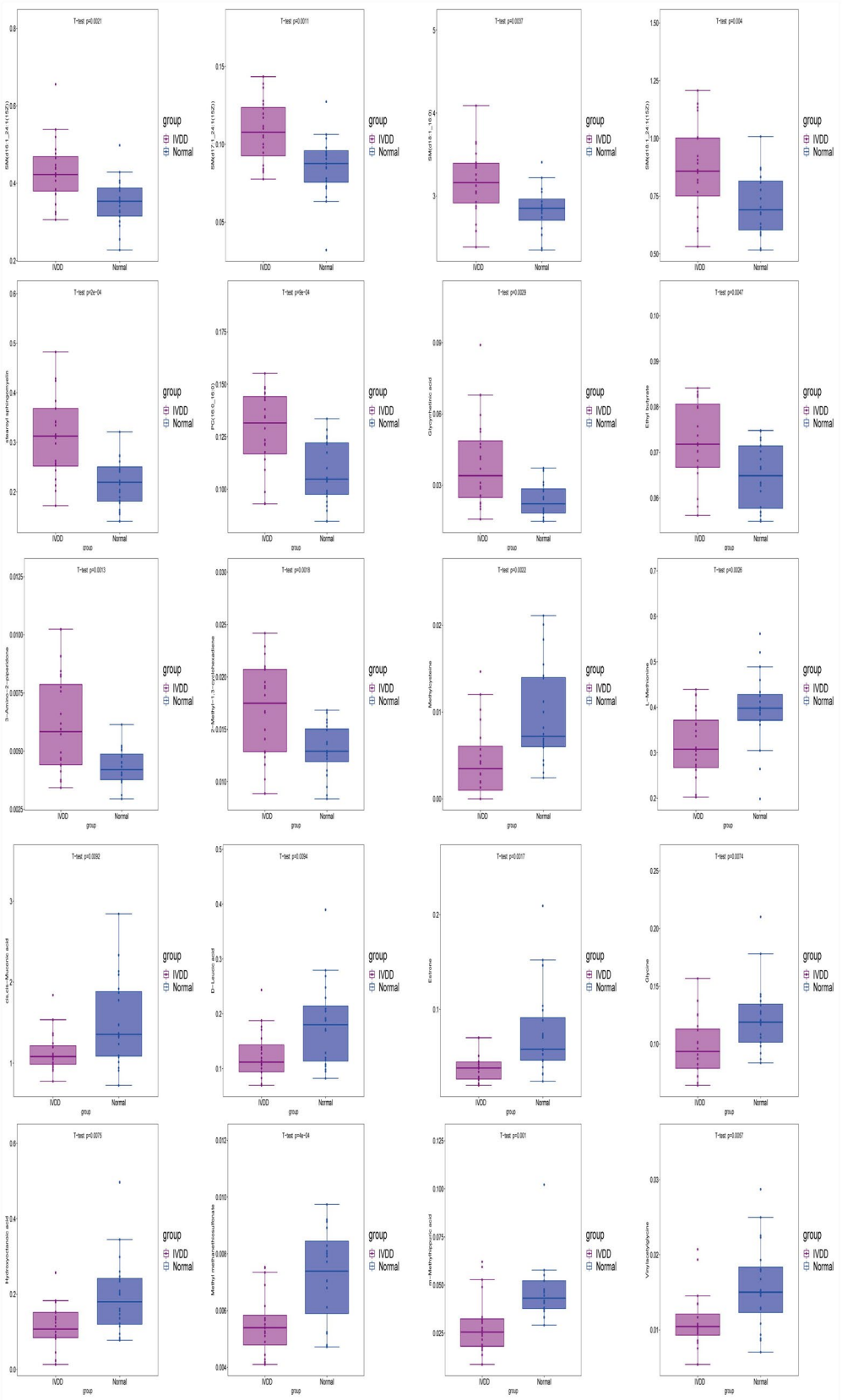

FIGURE 3 | The key differential metabolites between the control and IVDD groups.

categories and their content changes. By associating metabolite classification sources with differential metabolites, we calculated the correlation between them using the Spearman method and visualized the results in a chord diagram. This analysis provides deeper insights into the potential biological significance of changes in metabolite categories [28].

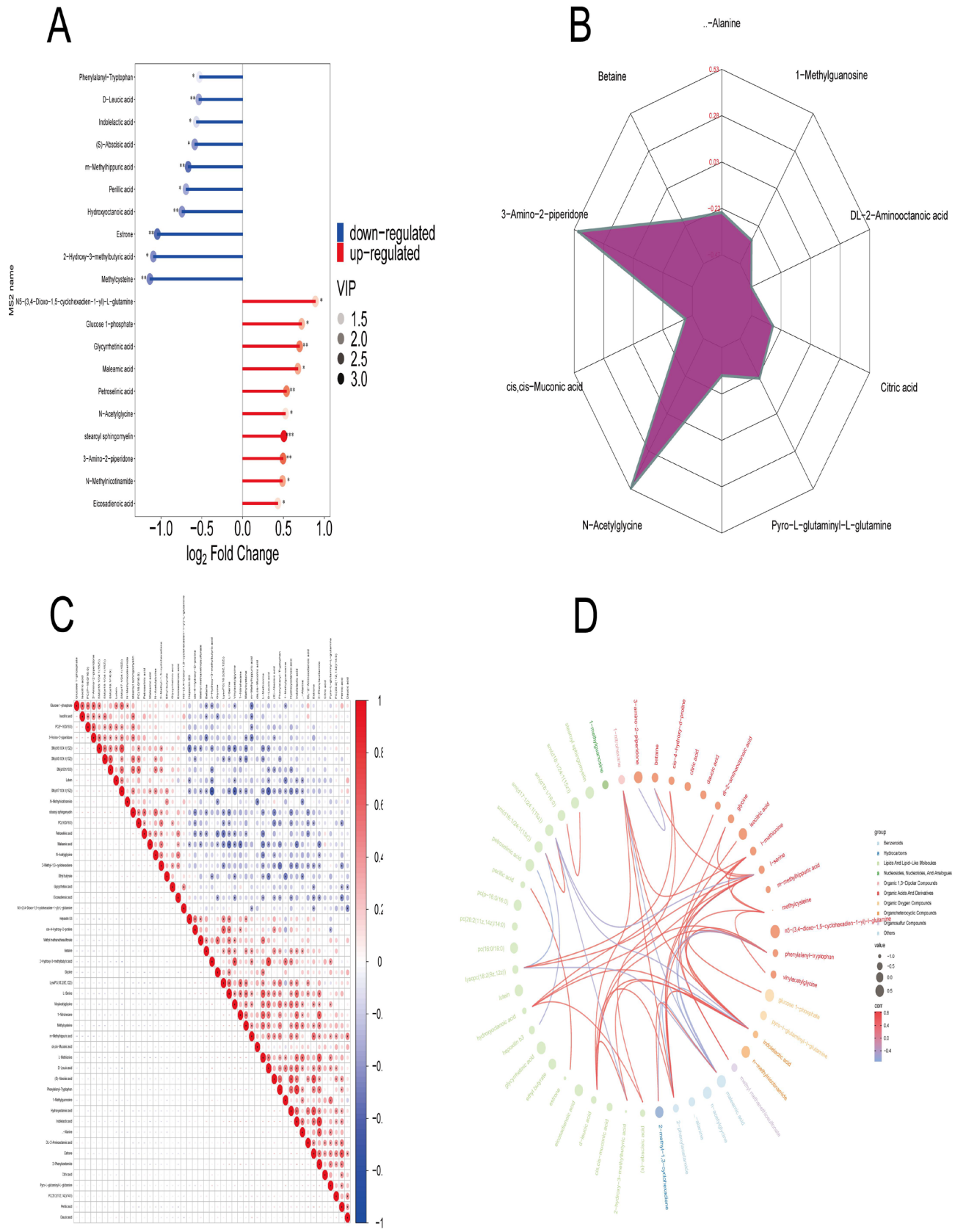

FIGURE 4 | Differential metabolite analysis in different ways. (A) The matchstick plot of differential metabolites. (B)The radargram analysis of differential metabolites. (C) Correlation analysis of differential metabolites. (D) Chordal analysis of differential metabolites.

3.5.3 | KEGG Annotation and Enrichment Analysis of Differential Metabolites

After obtaining the above results, we labeled the differential metabolites on the KEGG pathway map as shown in (Figure 5A), where dots indicate metabolites, bright red represents up-regulated significant differential metabolites, and bright blue represents down-regulated significant differential metabolites; boxes indicate genes (proteins) involved in the pathway; and the connecting lines indicate the flow direction of metabolic reactions. Categorized according to the results of KEGG pathway annotation, as shown in (Figure 5B).

3.5.4 | Differential Abundance Score

Differential Abundance Score (DA Score) is the ratio of the difference between the number of up-regulated and down-regulated differential metabolites annotated on a pathway to the number of all metabolites on that pathway, which serves to reflect the overall change of all differential metabolites in a pathway, DA Score is shown as (Figure 5C), the horizontal coordinate in the figure indicates the differential abundance score (DA Score), and the vertical coordinate indicates the name of KEGG metabolic pathway. DA Score reflects the overall change of all metabolites in a metabolic pathway, and a score of 1 indicates that the expression of all annotated differential metabolites in the pathway tends to be up-regulated, and −1 indicates that the expression of all annotated differential metabolites in the pathway tends to be down-regulated, and the length of the line segment represents the absolute value of the DA Score's absolute value. The size of the dots indicates the number of annotated differential metabolites in the pathway, and larger dots indicate more differential metabolites in the pathway. The longer the dots are distributed on the right side of the center axis, the more up-regulated the overall expression of the pathway is; the longer the dots are distributed on the left side of the center axis, the more down-regulated the overall expression of the pathway is.

3.5.5 | Metabolic Pathway Analysis of Differential Metabolites

By comprehensively analyzing the pathways where the differential metabolites are located, we aimed to further identify key pathways with the highest relevance to metabolite differences. Differential metabolites were mapped to authoritative metabolite databases such as KEGG and PubChem. Representative mapping results are provided in Table S2. After obtaining the matched metabolite information, we performed pathway analyses based on *Homo sapiens* (human) pathway databases. A metabolic pathway analysis table is provided in Table S3.

The results are visualized in a bubble plot (Figure 6A), where each bubble represents a metabolic pathway. The horizontal coordinates and size of the bubbles indicate the pathway's impact factor in topological analysis, with larger sizes corresponding to higher impact factors. The vertical coordinates and color of the bubbles reflect the p value of the enrichment analysis (negative natural logarithm, $-\ln(P)$), with darker colors indicating smaller p values and more significant enrichment. Pathways with larger, darker bubbles were identified as key pathways for further study. These key pathways were highlighted in the plot to allow intuitive identification.

To further diversify the presentation of metabolic changes, we transformed the bubble plot into a treemap plot (Figure 6B). Each square represents a metabolic pathway, with the size indicating the pathway's impact factor and the color representing the p value of enrichment analysis. Pathways with larger and darker squares were prioritized for detailed discussion.

3.5.6 | Regulatory Network Analysis of Differential Metabolites

Metabolic pathways represent series of biochemical reactions facilitated by enzymes, while metabolic networks illustrate the relationships between these reactions and regulatory mechanisms. Using the KEGG database for *H. sapiens*, we constructed network-based enrichment analyses (Figure 7). In these networks, red nodes represent metabolic pathways, yellow nodes indicate regulatory enzymes, green nodes denote background substances, purple nodes signify molecular modules, blue nodes represent chemical interactions, and green squares highlight the differential metabolites identified in this study. “Glycine, Serine, and Threonine Metabolism,” this pathway, highlighted in the abstract and introduction, plays a vital role in maintaining cellular redox balance and energy metabolism: SHMT facilitates the conversion of serine to glycine, generating tetrahydrofolate (THF), a critical component in one-carbon metabolism. Dysregulation of SHMT may enhance nucleic acid and protein synthesis, contributing to pathological tissue proliferation or metabolic imbalance. GLDC participates in glycine degradation and mitochondrial function regulation. Changes in GLDC activity may impact oxidative stress levels and energy metabolism, potentially exacerbating pathological conditions. Glycine is a precursor for glutathione (GSH) synthesis and plays a role in maintaining cellular redox balance. Glycine depletion may reduce antioxidant capacity, exacerbating oxidative stress and cellular dysfunction. Serine is crucial for phospholipid synthesis and membrane integrity. Dysregulation of serine metabolism may lead to impaired membrane function and increased inflammatory responses. Threonine degradation provides acetyl-CoA and succinyl-CoA, essential for energy production. Impaired threonine metabolism may contribute to energy deficits in affected tissues. Enhanced SHMT and GLDC activity in this pathway may represent a compensatory mechanism against oxidative stress. However, metabolite depletion (e.g., glycine) could weaken this defense, further aggravating pathological states. Altered production of key intermediates (e.g., acetyl-CoA) may disrupt the tricarboxylic acid cycle and mitochondrial function, impairing tissue repair and cell survival.

In this study, the significant alterations in “Glycine, Serine, and Threonine Metabolism” are closely related to the pathological state of the subject. Elevated SHMT or GLDC activity may indicate metabolic stress, while metabolite imbalances (e.g., glycine and serine) could serve as potential biomarkers for pathological progression.

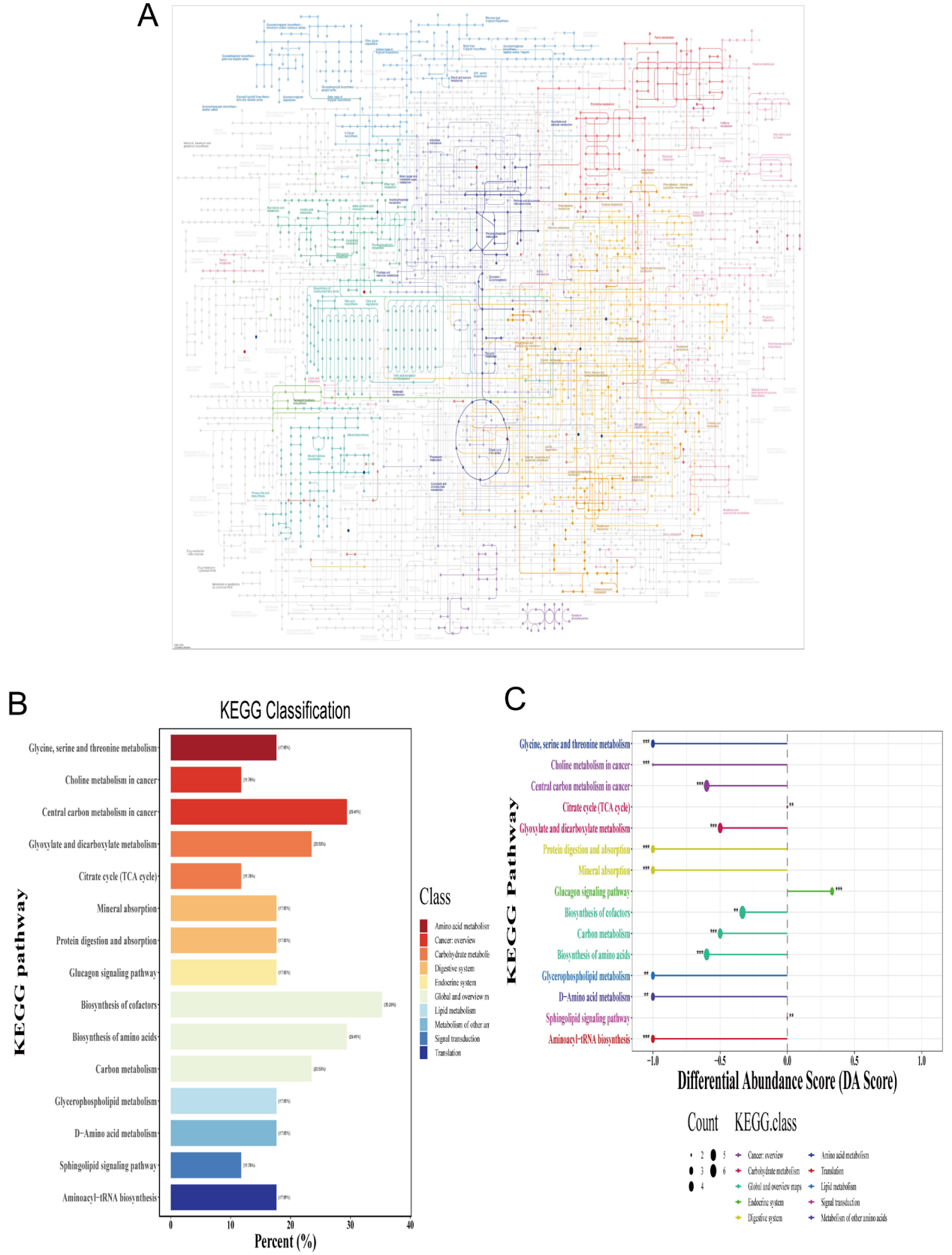

FIGURE 5 | KEGG analysis of differential metabolites. (A) KEGG pathway map of differential metabolites. (B) Categorized the results of KEGG pathway annotation. (C) Differential abundance score of KEGG metabolic pathways.

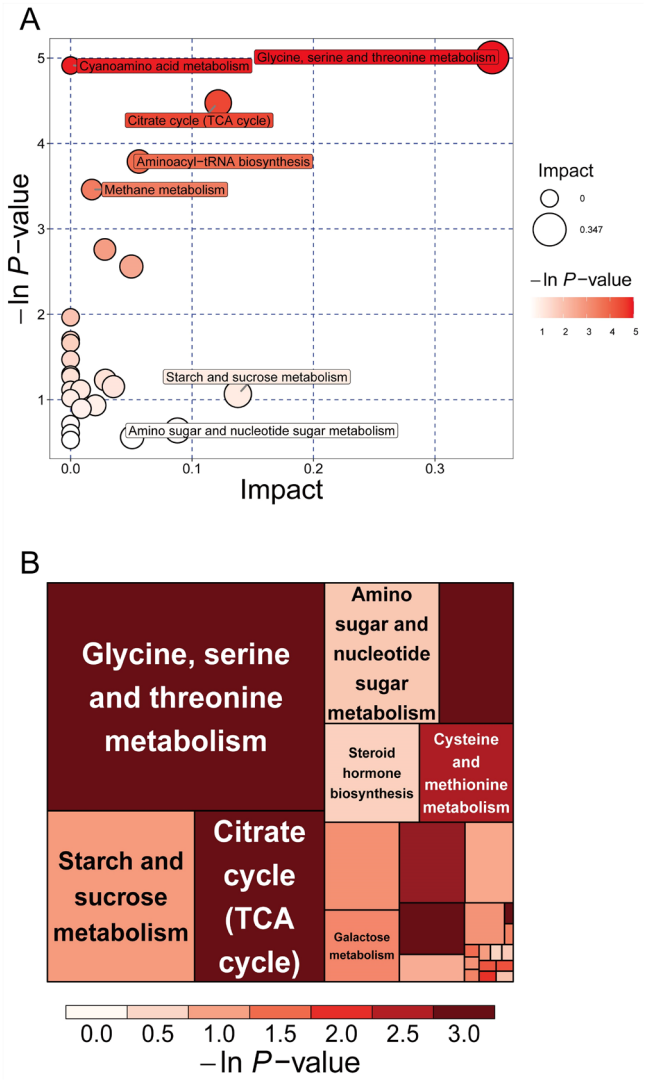

FIGURE 6 | Bubble plots and treemap of the pathway analysis. (A) Each bubble indicates a metabolic pathway. Control group vs. the IVDD group. (B) Each square in the rectangular tree diagram represents a metabolic pathway, and the size of the square indicates the magnitude of the pathway's influence factor in the topology analysis.

3.6 | ROC Analysis of Differential Metabolites

We plotted ROC curves for each clearly characterized differential metabolite and calculated its area under curve (AUC), with area under curve values between 1.0 and 0.5. In the case of AUC > 0.5, the closer the AUC is to 1, the better the diagnostic effect is. AUC in 0.5 ~ 0.7 is with lower accuracy, AUC in 0.7 ~ 0.9 has some accuracy, AUC in 0.9 and above has higher accuracy. AUC = 0.5 indicates that the diagnostic method does not work at all, and has no diagnostic value. As shown in (Figure 8), all metabolites in the figure have high diagnostic value.

4 | Discussion

With the aging of the population and the impact of long office hours, IVDD will inevitably become a common and frequent disease of great concern nowadays and even in the future [29], and the LBP it causes is one of the main causes of disability, which imposes a heavy economic burden and social pressure on the patient's family [30]. As a key research area of orthopedic diseases, IVDD has limited therapeutic options. The fundamental reason is that the pathophysiologic mechanisms of IVDD are not fully understood [31]. The flourishing of metabolomics has facilitated a more in-depth understanding of the pathogenesis of the disease [32]. In this study, based on untargeted metabolomics, we explored the changes of differential metabolites in the normal control group ($n = 20$) and the disease group of IVDD patients ($n = 20$), moving forward from previous knowledge on metabolite levels in plasma from patients [33], and identified some metabolites and metabolic pathways that play a key role in the pathogenesis of IVDD, which is conducive to further understanding the pathophysiological mechanisms in the development of IVDD. A total of 2-methyl-1,3-cyclohexadiene, 3-amino-2-piperidone, ethyl butyrate, glycyrrhetinic acid, SM(d16:1/24:1), SM(d17:1/24:1), SM(d18:1/16:0), SM(d18:1/24:1), stearoyl sphingomyelin and other metabolites are on the rise in patients with IVDD, methylcysteine, L-methionine, cis, cis-muconic acid, estrone, glycine, hydroxyoctanoic acid, methyl methanethiosulfonate, m-methylhippuric acid, and vinylacetylglycine metabolites showed a decreasing trend, which was suggested by KEGG analysis to be related with glycine, serine and threonine metabolism, cyanoamino acid metabolism, citrate cycle (TCA cycle), aminoacyl-tRNA biosynthesis, methane metabolism. Glyoxylate and dicarboxylate metabolism, cysteine and methionine metabolism and other pathways are closely linked.

It is worth focusing on the fact that lipids and lipid-like molecules accounted for 44.9% and organic acids and derivatives accounted for 30.61%. Among the metabolites that showed an increasing trend in IVDD patients, SM(d16_1 SM(d16_1_24_1(15Z))), SM(d17_1_24_1(15Z)), SM(d18_1_16_0), SM(d18_1_24_1(15Z)), and stearoyl sphingomyelin all belong to sphingolipids, and sphingolipids are lipids with a special structure called "sphingolipid base." Sphingolipids are lipids with a special structure called "sphingolipid base," and sphingolipids are not only essential membrane components but also bioactive lipid mediators that regulate many biological functions [34]. The regulation of ceramide levels in cells depends on many sphingolipid metabolizing enzymes such as sphingomyelinase (SMase), sphingomyelin synthase (SMS), ceramidase, and ceramide synthase. Ceramides induce many types of cell death such as apoptosis, necrosis, iron death and autophagy-regulated cell death; senescence; differentiation; and autophagy as a lipid mediator [35]. Sphingomyelin (SM) is generated by the transfer of phosphorylcholine to ceramides via SMSs and is also an important membrane component anatomically and biologically, with SM in cell membranes localized in restricted regions called "SM-rich microdomains," which provide a specific environment to regulate the binding of ligands to their receptors to express cellular functions, including proliferation, migration and inflammation. This region provides a specific environment to regulate the binding of ligands to their receptors in order to express cellular functions, including proliferation, migration and inflammation [36]. Numerous studies have shown that SM-rich microdomains regulated by SMS play a key role as membrane platforms for numerous receptors such as T-cell receptor (TCR), TNF receptor, toll-like receptor, and C-X-C chemokine receptor type 4 (CXCR4), such as transduction of proliferative, migratory,

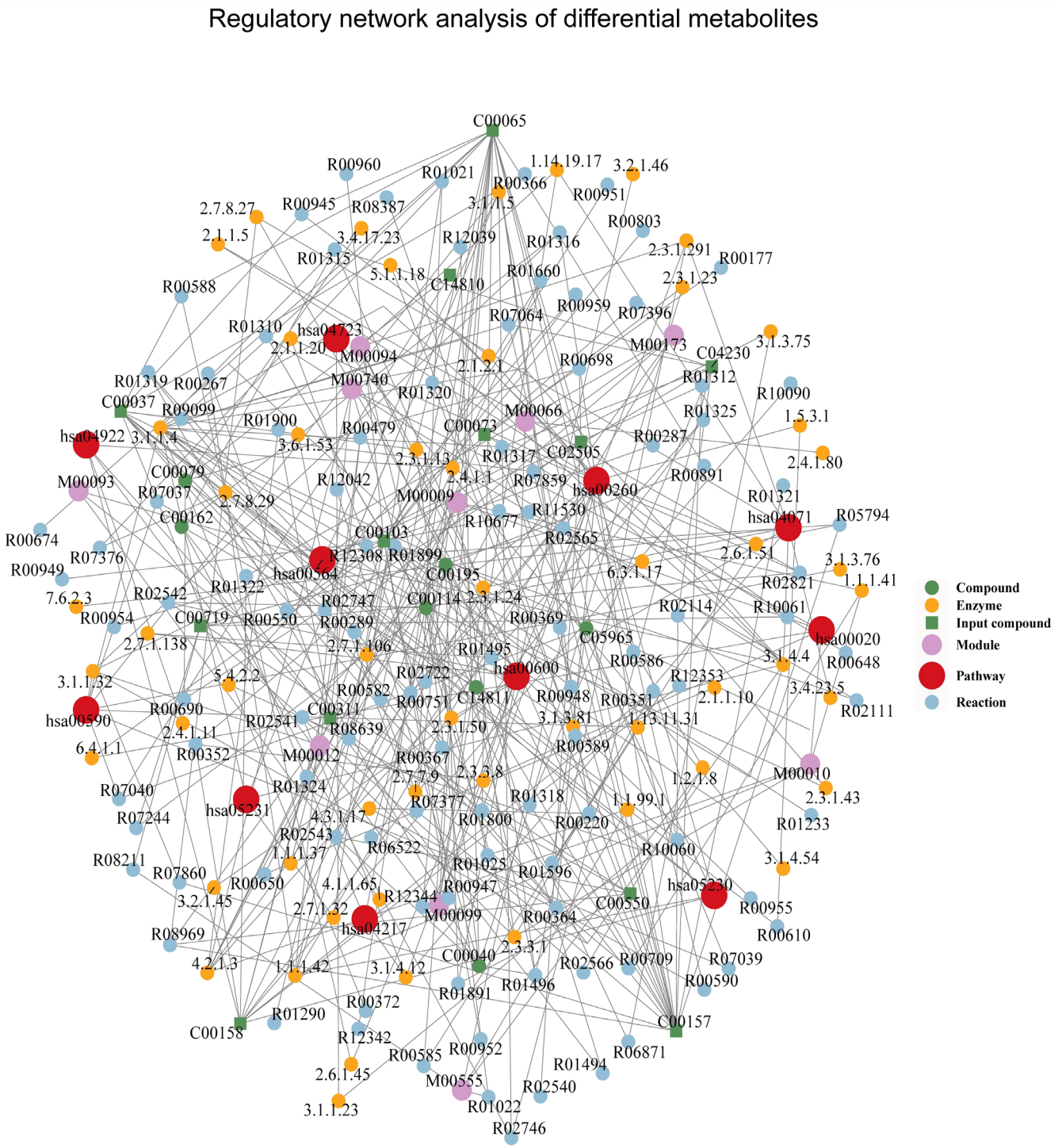

FIGURE 7 | Regulatory network analysis of differential metabolites. Red dots represent a metabolic pathway, the yellow dots represent information of a substance-associated regulatory enzyme, the green dots represent the background substance of a metabolic pathway, and the purple dots represent information of molecular modules of a class of substances, blue dots represent chemical interactions of a substance, and green squares represent differential substances obtained from this comparison.

and inflammatory signals. In addition, ceramide transforms SM-rich microstructural domains via SMase to form ceramide-rich platforms that regulate cellular functions by recruiting and aggregating receptors or altering membrane properties [37–42]. In summary, it is highly likely that the SM/ceramide cycle imbalance caused by elevated SM in patients with disc degeneration plays an important role in the IVDD process. In addition, it has been shown that metabolites such as 2-methyl-1,3-cyclohexadiene, 3-amino-2-piperidone, ethyl butyrate, glycyrrhetinic acid, and SM (d16:1/24:1) are also elevated in patients with IVDD, and that the remaining in patients with disc degeneration The specific role of elevated metabolites remains to be further explored.

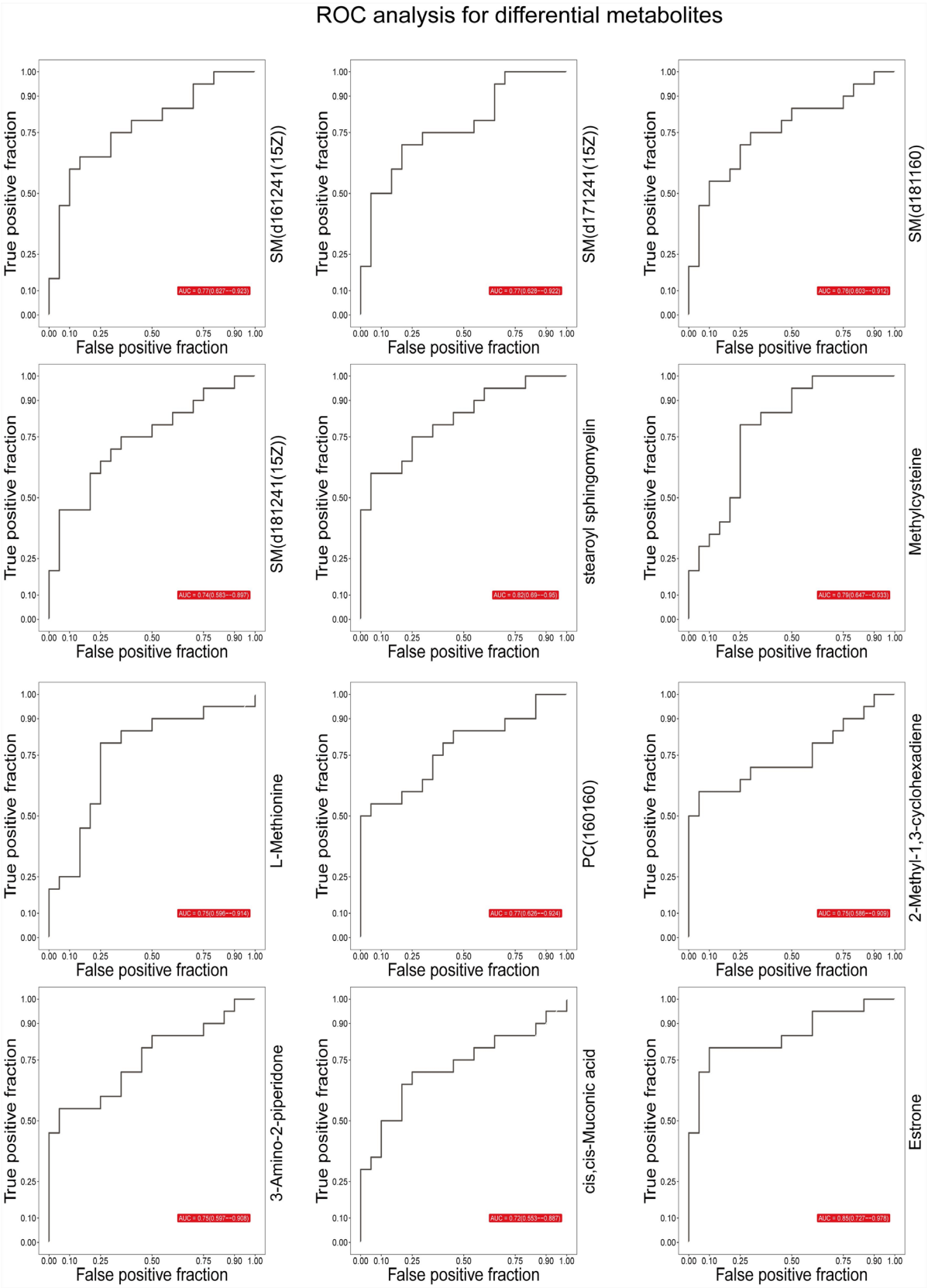

FIGURE 8 | ROC analysis of differential metabolites. AUC of 0.5~0.7 has low accuracy, AUC of 0.7~0.9 has some accuracy, and AUC of more than 0.9 has high accuracy.

In addition to this, our study found that methylcysteine, L-methionine was down-regulated in patients with disc degeneration, and cysteine has the function of regulating glutathione synthesis. Glutathione is an important antioxidant and oxygen radical scavenger in the body. Methionine is involved in the destruction of membrane lipids generated by oxidizing free radicals through various oxidative pathways, thus protecting membrane structures such as cells and mitochondria [43]. Down-regulation of cysteine and methionine metabolism during the development of disc degeneration leads to a decrease in the antioxidant function of the intradiscal environment [44], whereas the peroxidized environment within the disc leads to an increase in reactive oxygen species (ROS), which promotes senescence, apoptosis, and scorched death of the nucleus pulposus cells (NPCs), and exacerbates the degree of disc degeneration [6, 45].

What is worth focusing on in the pathway is that the TCA cycle is the final metabolic pathway and metabolic hub for Sphingomyelin the three major nutrients [46]. Sphingomyelin, a critical component of cell membranes, plays a significant role in maintaining cellular integrity and signaling. Recent studies have implicated sphingomyelin in inflammation-related pathways, such as the activation of pro-inflammatory cytokines and modulation of immune cell responses. However, its specific contribution to IVDD remains unclear. Our findings suggest alterations in sphingomyelin levels in IVDD patients, which may be linked to the dysregulation of inflammatory pathways or oxidative stress mechanisms. While this provides preliminary evidence for its involvement, further research is needed to elucidate the precise molecular mechanisms by which sphingomyelin influences IVDD pathogenesis. Such studies could enhance our understanding of the disease and identify potential therapeutic targets. Downregulation of the TCA cycle in the late stages of disc degeneration implies that the metabolites of IVDD are depleted, which is attributed to the apoptosis of NP cells and their decreased secretory function. In addition, it has been shown that the process of IVDD is closely related to the functional state of the Gly–Ser–Thr metabolic axis, which is involved in biotransformation and metabolic activities during degeneration, and that antioxidants are produced through the Gly–Ser–Thr metabolic axis. The Gly–Ser–Thr metabolic axis may be involved in IVDD by regulating carbohydrate onversion and energy utilization and ultimately retarding IVDD degeneration through the formation of antioxidants [47, 48]. In summary, the TCA cycle and the Gly–Ser–Thr metabolic pathway may play an extremely important role in IVDD. The association of the remaining pathways with IVDD and the related mechanisms still need to be explored and verified by further studies, and in-depth studies can help to provide new directions and strategies for the treatment and prevention of IVDD.

5 | Conclusion

Based on our findings, we successfully identified differential metabolites and related pathways associated with IVDD using ultra-high-performance liquid chromatography-mass spectrometry (UHPLC-MS). These metabolites were further analyzed using the Kyoto Encyclopedia of Genes and Genomes (KEGG) database to determine relevant pathways.

Key metabolites, including sphingomyelins include SM(d16:1/24:1), SM(d17:1/24:1), SM(d18:1/16:0), SM(d18:1/24:1), and methylcysteine, L-methionine, glycine, and citrate cycle intermediates, were found to be significantly altered. KEGG analysis suggested that these metabolites are involved in pathways such as glycine, serine, and threonine metabolism, the citrate cycle (TCA cycle), aminoacyl-tRNA biosynthesis, and cysteine and methionine metabolism.

These findings provide valuable insights into the pathogenesis of IVDD. Metabolites such as sphingomyelin and pathways like the citrate cycle and glycine–serine–threonine metabolism may play key regulatory roles in IVDD development. This study enhances our understanding of the pathophysiological processes underlying IVDD and identifies potential targets for future clinical diagnosis and therapeutic strategies.

Author Contributions

Conceptualization: Z.L. Data curation: X.Z. Formal analysis: Y.L. and F.L. Methodology: D.Z. Visualization: J.L. Writing – original draft: D.Z. Review and editing: Y.M.

Ethics Statement

The study was reviewed and approved by the Medical Ethics Committee of the Affiliated Hospital of Traditional Chinese Medicine of Southwest Medical University [KY2021051-FS01].

Consent

Informed consent was obtained from all individual participants included in the study.

Conflicts of Interest

The authors declare no conflicts of interest.

Data Availability Statement

The datasets used and/or analyzed during the current study available from the corresponding author on reasonable request.

References

1. Y. Shao, L. Sun, G. Yang, et al., "Icariin Protects Vertebral Endplate Chondrocytes Against Apoptosis and Degeneration via Activating Nrf-2/HO-1 Pathway," *Frontiers in Pharmacology* 13 (2022): 937502.

2. A. Dower, M. A. Davies, and A. Ghahreman, "Pathologic Basis of Lumbar Radicular Pain," *World Neurosurgery* 128 (2019): 114–121.

3. X. Yang, D. S. A. Karis, and C. L. A. Vleggeert-Lankamp, "Association Between Modic Changes, Disc Degeneration, and Neck Pain in the Cervical Spine: A Systematic Review of Literature," *Spine Journal* 20, no. 5 (2020): 754–764.

4. I. Cosamalón-Gan, T. Cosamalón-Gan, G. Mattos-Piaggio, V. Villar-Suárez, J. García-Cosamalón, and J. A. Vega-Álvarez, "Inflammation in the Intervertebral Disc Herniation," *Neurocirugía (English Edition)* 32, no. 1 (2021): 21–35.

5. C. Feng, M. Yang, M. Lan, et al., "ROS: Crucial Intermediators in the Pathogenesis of Intervertebral Disc Degeneration," *Oxidative Medicine and Cellular Longevity* 2017 (2017): 5601593.

6. D. Zhou, C. Song, Y. Mei, et al., "A Review of Duhuo Jisheng Decoction Mechanisms in Intervertebral Disc Degeneration In Vitro and Animal Studies," *Journal of Orthopaedic Surgery and Research* 18, no. 1 (2023): 436.

7. L. Wang, Q. Guo, X. Lu, and B. Ni, "Surgical Versus Nonsurgical Treatment of Chronic Low Back Pain: A Meta-Analysis Based on Current Evidence," *Journal of Back and Musculoskeletal Rehabilitation* 29, no. 3 (2016): 393–401.

8. U. H. Mitchell, K. Helgeson, and P. Mintken, "Physiological Effects of Physical Therapy Interventions on Lumbar Intervertebral Discs: A Systematic Review," *Physiotherapy Theory and Practice* 33, no. 9 (2017): 695–705.

9. C. Maher, M. Underwood, and R. Buchbinder, "Non-Specific Low Back Pain," *Lancet* 389, no. 10070 (2017): 736–747.

10. M. Arita, "What Can Metabolomics Learn From Genomics and Proteomics?," *Current Opinion in Biotechnology* 20, no. 6 (2009): 610–615.

11. R. Tan, S. Ou, T. Kang, et al., "Altered Serum Metabolome Associated With Vascular Calcification Developed From CKD and the Critical Pathways," *Frontiers in Cardiovascular Medicine* 10 (2023): 1114528.

12. J. F. Griffith, Y. X. J. Wang, G. E. Antonio, et al., "Modified Pfirrmann Grading System for Lumbar Intervertebral Disc Degeneration," *Spine (Phila Pa 1976)* 32, no. 24 (2007): E708–E712.

13. C. W. Pfirrmann, A. Metzdorf, M. Zanetti, J. Hodler, and N. Boos, "Magnetic Resonance Classification of Lumbar Intervertebral Disc Degeneration," *Spine (Phila Pa 1976)* 26, no. 17 (2001): 1873–1878.

14. W. H. Kirkaldy-Willis and H. F. Farfan, "Instability of the Lumbar Spine," *Clinical Orthopaedics and Related Research* 165 (1982): 110–123.

15. X. Chen, K. Chen, J. Hu, et al., "Multiomics Analysis Reveals the Potential of LPCAT1-PC Axis as a Therapeutic Target for Human Intervertebral Disc Degeneration," *International Journal of Biological Macromolecules* 276, no. Pt 1 (2024): 133779.

16. V. Francisco, D. Ait Eldjoudi, M. González-Rodríguez, et al., "Metabolomic Signature and Molecular Profile of Normal and Degenerated Human Intervertebral Disc Cells," *Spine Journal* 23, no. 10 (2023): 1549–1562.

17. W. B. Dunn, D. Broadhurst, P. Begley, et al., "Procedures for Large-Scale Metabolic Profiling of Serum and Plasma Using Gas Chromatography and Liquid Chromatography Coupled to Mass Spectrometry," *Nature Protocols* 6, no. 7 (2011): 1060–1083.

18. J. L. Wang, T. Zhang, X. Shen, et al., "Serum Metabolomics for Early Diagnosis of Esophageal Squamous Cell Carcinoma by UHPLC-QTOF/MS," *Metabolomics* 12, no. 7 (2016): 3944–3957.

19. X. Domingo-Almenara, J. R. Montenegro-Burke, H. P. Benton, and G. Siuzdak, "Annotation: A Computational Solution for Streamlining Metabolomics Analysis," *Analytical Chemistry* 90, no. 1 (2018): 480–489.

20. C. A. Smith, E. J. Want, G. O'Maille, R. Abagyan, and G. Siuzdak, "XCMS: Processing Mass Spectrometry Data for Metabolite Profiling Using Nonlinear Peak Alignment, Matching, and Identification," *Analytical Chemistry* 78, no. 3 (2006): 779–787.

21. M. Ringnér, "What Is Principal Component Analysis?," *Nature Biotechnology* 26, no. 3 (2008): 303–304.

22. S. Wiklund, E. Johansson, L. Sjöström, et al., "Visualization of GC/TOF-MS-Based Metabolomics Data for Identification of Biochemically Interesting Compounds Using OPLS Class Models," *Analytical Chemistry* 80, no. 1 (2008): 115–122.

23. U. G. Indahl, "The O-PLS Methodology for Orthogonal Signal Correction-Is It Correcting or Confusing?," *Journal of Chemometrics* 34, no. 1 (2020): e2884.

24. B. Worley and R. Powers, "Multivariate Analysis in Metabolomics," *Current Metabolomics* 1, no. 1 (2013): 92–107.

25. M. N. Triba, L. le Moyec, R. Amathieu, et al., "PLS/OPLS Models in Metabolomics: The Impact of Permutation of Dataset Rows on the K-Fold Cross-Validation Quality Parameters," *Molecular BioSystems* 11, no. 1 (2015): 13–19.

26. H. Ogata, S. Goto, K. Sato, W. Fujibuchi, H. Bono, and M. Kanehisa, "KEGG: Kyoto Encyclopedia of Genes and Genomes," *Nucleic Acids Research* 27, no. 1 (1999): 29–34.

27. J. Benesty, J. D. Chen, and Y. T. Huang, "On the Importance of the Pearson Correlation Coefficient in Noise Reduction," *IEEE Transactions on Audio Speech and Language Processing* 16, no. 4 (2008): 757–765.

28. S. N. Reinke, B. Galindo-Prieto, T. Skotare, et al., "OnPLS-Based Multi-Block Data Integration: A Multivariate Approach to Interrogating Biological Interactions in Asthma," *Analytical Chemistry* 90, no. 22 (2018): 13400–13408.

29. F. Wang, F. Cai, R. Shi, X. H. Wang, and X. T. Wu, "Aging and Age Related Stresses: A Senescence Mechanism of Intervertebral Disc Degeneration," *Osteoarthritis and Cartilage* 24, no. 3 (2016): 398–408.

30. GBD 2017 Disease and Injury Incidence and Prevalence Collaborators, "Global, Regional, and National Incidence, Prevalence, and Years Lived With Disability for 354 Diseases and Injuries for 195 Countries and Territories, 1990-2017: A Systematic Analysis for the Global Burden of Disease Study 2017," *Lancet* 392, no. 10159 (2018): 1789–1858.

31. C. Song, W. Cai, F. Liu, K. Cheng, D. Guo, and Z. Liu, "An In-Depth Analysis of the Immunomodulatory Mechanisms of Intervertebral Disc Degeneration," *JOR Spine* 5, no. 4 (2022): e1233.

32. R. Wang, B. Li, S. M. Lam, and G. Shui, "Integration of Lipidomics and Metabolomics for In-Depth Understanding of Cellular Mechanism and Disease Progression," *Journal of Genetics and Genomics* 47, no. 2 (2020): 69–83.

33. K. R. Swank, J. E. Furness, E. A. Baker, C. K. Gehrke, S. P. Biebelhausen, and K. C. Baker, "Metabolomic Profiling in the Characterization of Degenerative Bone and Joint Diseases," *Metabolites* 10, no. 6 (2020): 223.

34. Y. A. Hannun and L. M. Obeid, "Sphingolipids and Their Metabolism in Physiology and Disease," *Nature Reviews. Molecular Cell Biology* 19, no. 3 (2018): 175–191.

35. M. Heinrich, M. Wickel, W. Schneider-Brachert, et al., "Cathepsin D Targeted by Acid Sphingomyelinase-Derived Ceramide," *EMBO Journal* 18, no. 19 (1999): 5252–5263.

36. M. Taniguchi and T. Okazaki, "Ceramide/Sphingomyelin Rheostat Regulated by Sphingomyelin Synthases and Chronic Diseases in Murine Models," *Journal of Lipid and Atherosclerosis* 9, no. 3 (2020): 380–405.

37. Z. X. Jin, C. R. Huang, L. Dong, et al., "Impaired TCR Signaling Through Dysfunction of Lipid Rafts in Sphingomyelin Synthase 1 (SMS1)-Knockdown T Cells," *International Immunology* 20, no. 11 (2008): 1427–1437.

38. L. Dong, K. Watanabe, M. Itoh, et al., "CD4+ T-Cell Dysfunctions Through the Impaired Lipid Rafts Ameliorate Concanavalin A-Induced Hepatitis in Sphingomyelin Synthase 1-Knockout Mice," *International Immunology* 24, no. 5 (2012): 327–337.

39. T. K. Hailemariam, C. Huan, J. Liu, et al., "Sphingomyelin Synthase 2 Deficiency Attenuates NFkappaB Activation," *Arteriosclerosis, Thrombosis, and Vascular Biology* 28, no. 8 (2008): 1519–1526.

40. J. Xue, Y. Yu, X. Zhang, et al., "Sphingomyelin Synthase 2 Inhibition Ameliorates Cerebral Ischemic Reperfusion Injury Through Reducing the Recruitment of Toll-Like Receptor 4 to Lipid Rafts," *Journal of the American Heart Association* 8, no. 22 (2019): e012885.

41. S. Asano, K. Kitatani, M. Taniguchi, et al., "Regulation of Cell Migration by Sphingomyelin Synthases: Sphingomyelin in Lipid Rafts Decreases Responsiveness to Signaling by the CXCL12/CXCR4 Pathway," *Molecular and Cellular Biology* 32, no. 16 (2012): 3242–3252.

42. B. Stancevic and R. Kolesnick, "Ceramide-Rich Platforms in Transmembrane Signaling," *FEBS Letters* 584, no. 9 (2010): 1728–1740.

43. C. Ye, B. M. Sutter, Y. Wang, Z. Kuang, and B. P. Tu, "A Metabolic Function for Phospholipid and Histone Methylation," *Molecular Cell* 66, no. 2 (2017): 180–193.e8.

44. M. Sohail, R. B. H. Wills, M. C. Bowyer, and P. Pristijono, "Beneficial Impact of Exogenous Arginine, Cysteine and Methionine on Postharvest Senescence of Broccoli," *Food Chemistry* 338 (2021): 128055.

45. C. Song, Y. Zhou, K. Cheng, et al., "Cellular Senescence—Molecular Mechanisms of Intervertebral Disc Degeneration From an Immune Perspective," *Biomedicine & Pharmacotherapy* 162 (2023): 114711.

46. J. Xu, Y. Zhai, L. Feng, et al., "An Optimized Analytical Method for Cellular Targeted Quantification of Primary Metabolites in Tricarboxylic Acid Cycle and Glycolysis Using Gas Chromatography-Tandem Mass Spectrometry and Its Application in Three Kinds of Hepatic Cell Lines," *Journal of Pharmaceutical and Biomedical Analysis* 171 (2019): 171–179.

47. M. A. Aon, M. Bernier, S. J. Mitchell, et al., "Untangling Determinants of Enhanced Health and Lifespan Through a Multi-Omics Approach in Mice," *Cell Metabolism* 32, no. 1 (2020): 100–116.e4.

48. X. Wu, C. Liu, S. Yang, et al., "Glycine-Serine-Threonine Metabolic Axis Delays Intervertebral Disc Degeneration Through Antioxidant Effects: An Imaging and Metabonomics Study," *Oxidative Medicine and Cellular Longevity* 2021 (2021): 5579736.

Supporting Information

Additional supporting information can be found online in the Supporting Information section.